Centriolar Satellites: Molecular Characterization, ATP-dependent Movement Toward Centrioles and Possible Involvement in Ciliogenesis✪

Akiharu Kubo,*‡§ Hiroyuki Sasaki,‖¶ Akiko Yuba-Kubo,* Shoichiro Tsukita,*‡ and Nobuyuki Shiina*

*Tsukita Cell Axis Project, Exploratory Research for Advanced Technology, Japan Science and Technology Corporation, Kyoto Research Park, Shimogyo-ku, Kyoto 600-8813, Japan; ‡Department of Cell Biology, Kyoto University Faculty of Medicine, Sakyo-ku, Kyoto 606-8501, Japan; §Department of Dermatology, Osaka University School of Medicine, Suita 565-0871, Japan; ‖Laboratory of Cell Biology, KAN Research Institute Inc., Kyoto Research Park, Shimogyo-ku, Kyoto 600-8815, Japan; and ¶Department of Molecular Cell Biology, Institute of DNA Medicine, Jikei University School of Medicine, Minato-ku, Tokyo 105-0003, Japan

Abstract. We identified *Xenopus* pericentriolar material-1 (PCM-1), which had been reported to constitute pericentriolar material, cloned its cDNA, and generated a specific pAb against this molecule. Immunolabeling revealed that PCM-1 was not a pericentriolar material protein, but a specific component of centriolar satellites, morphologically characterized as electron-dense granules, ~70–100 nm in diameter, scattered around centrosomes. Using a GFP fusion protein with PCM-1, we found that PCM-1–containing centriolar satellites moved along microtubules toward their minus ends, i.e., toward centrosomes, in live cells, as well as in vitro reconstituted asters. These findings defined centriolar satellites at the molecular level, and explained their pericentriolar localization. Next, to understand the relationship between centriolar satellites and centriolar replication, we examined the expression and subcellular localization of PCM-1 in ciliated epithelial cells during ciliogenesis. When ciliogenesis was induced in mouse nasal respiratory epithelial cells, PCM-1 immunofluorescence was markedly elevated at the apical cytoplasm. At the electron microscopic level, anti–PCM-1 pAb exclusively labeled fibrous granules, but not deuterosomes, both of which have been suggested to play central roles in centriolar replication in ciliogenesis. These findings suggested that centriolar satellites and fibrous granules are identical novel nonmembranous organelles containing PCM-1, which may play some important role(s) in centriolar replication.

Key words: centriole • centriolar satellites • fibrous granule • pericentriolar material-1 • ciliogenesis

THE centrosome functions as an organizing center for cytoskeletal components, especially microtubules (MTs)[1] (Kimble and Kuriyama, 1992; Kalt and Schliwa, 1993; Kellogg et al., 1994; Zimmerman et al., 1999). This structure usually has a centriole pair at its center, surrounded by fibrous material known as the pericentriolar material. In addition to these structures, early electron microscopic observations identified electron-dense spherical granules, ~70–100 nm in diameter, localized around centrosomes in many types of vertebrate cells (Bernhard and De Harven, 1960; de-Thé, 1964; Berns et al., 1977; Rattner, 1992). These granules have been termed massules (Bessis and Breton-Gorius, 1958) or satellites (Bernhard and De Harven, 1960). They were occasionally shown to be associated with MTs radiating from centrosomes (de-Thé, 1964), and their number decreased and increased during mitosis and interphase, respectively (Rattner, 1992). However, mainly due to the lack of information regarding their molecular components, these granular structures have since attracted little attention.

The molecular mechanism behind the replication of centrosomes has attracted increasing interest (for reviews see Marshall and Rosenbaum, 1999; Zimmerman et al., 1999). At the G1/S transition, nascent centrioles appear and grow perpendicularly on the side of mother centrioles. Although in most cells, centrosomes are duplicated once per cell cycle, in ciliated epithelial cells, each of which bears

✪The online version of this article contains supplemental material.

Address correspondence to Nobuyuki Shiina, Tsukita Cell Axis Project, Exploratory Research for Advanced Technology, Japan Science and Technology Corporation, Kyoto Research Park, 17 Chudojiminami-machi, Shimogyo-ku, Kyoto 600-8813, Japan. Tel.: 81 (75) 315-7912. Fax: 81 (75) 315-6420. E-mail: nshiina@cell.tsukita.jst.go.jp

1. *Abbreviations used in this paper:* aa, amino acids; AMP-PNP, adenylylimido diphosphate; GFP, green fluorescent protein; MT, microtubule; ORF, open reading frame; pAb, polyclonal antibody; PCM-1, pericentriolar material-1.

hundreds of basal bodies, i.e., centrioles (Rhodin and Dalhamn, 1956), numerous replicating centrioles were simultaneously observed during ciliogenesis (Sorokin, 1968; Steinman, 1968; Anderson and Brenner, 1971; Dirksen, 1991). Therefore, ciliogenesis was thought to provide an advantageous system to examine the molecular mechanism of centriolar replication. Conventional ultrathin EM identified two distinct pathways for ciliogenesis in ciliated cells: centriolar and acentriolar pathways (Anderson and Brenner, 1971). In the centriolar pathway, multiple daughter centrioles grow out from mother centrioles, but this pathway appears to explain only a small fraction of centriolar replication during ciliogenesis (Anderson and Brenner, 1971). The acentriolar pathway is now thought to be more dominant for basal body replication. When ciliogenesis is induced in ciliated epithelial cells, so-called fibrous granules (Anderson and Brenner, 1971), nonmembranous electron-dense granules, ~70–100 nm in diameter, first appear in the cytoplasm (Sorokin, 1968; Steinman, 1968; Anderson and Brenner, 1971; Dirksen, 1991). These granules occasionally aggregate together with fibrous materials to form a fibrogranular area in the apical cytoplasm of ciliogenic cells. In the next step, deuterosomes (Sorokin, 1968), larger nonmembranous electron-dense spherical structures (~75–400 nm in diameter), appear within or close to the fibrogranular area. There is debate over whether deuterosomes are generated by aggregation and fusion of fibrous granules (Sorokin, 1968; Anderson and Brenner, 1971; Youson, 1982; Dirksen, 1991) or independently from fibrous granules (Loots and Nel, 1989). Multiple procentrioles grow out from deuterosomes, and mature daughter centrioles are separated from deuterosomes to travel toward the apical region where centrioles function as ciliary basal bodies. The binding of basal bodies to the plasma membrane then appears to initiate the elongation of axoneme. Interestingly, fibrous granules also exist around basal bodies during the elongation of axoneme (Steinman, 1968). The lack of information of the molecular components of these fibrous granules, as well as deuterosomes, however, has hampered the direct assessment of identity and functions of these structures in multiple centriolar replication and axonemal elongation during ciliogenesis.

During the course of our studies to identify centrosome-specific molecules in *Xenopus* oocytes, we identified the *Xenopus* homologue of pericentriolar material-1 (PCM-1) with a molecular mass of ~230 kD (Balczon et al., 1994). This molecule was initially identified as an antigen of human autoimmune sera. In HeLa cells, PCM-1 was reported to be associated with centrosomes in interphase, but dissociated in metaphase (Balczon et al., 1994). In this study, we identified PCM-1 as the first component of centriolar satellites, and found that PCM-1–containing centriolar satellites moved along MTs toward centrosomes in an ATP-dependent manner. Furthermore, we showed that PCM-1 was also concentrated in fibrous granules, but not in deuterosomes, in ciliogenic cells. These findings indicated the existence of a novel type of nonmembranous organelle containing PCM-1, previously called centriolar satellites or fibrous granules, and suggested the possible association of these organelles with centriolar replication.

Materials and Methods

Generation of Monoclonal Antibodies

Centrosomes were isolated from mouse L5178Y cells and treated with 1 M KCl (Ohta et al., 1993). *Xenopus* egg extracts were prepared as described previously (Shiina et al., 1992). Centrosomes (1 ml) were incubated with *Xenopus* egg extracts (5 ml) for 30 min at 20°C. After dilution with 15 ml of buffer A (10 mM Pipes, pH 7.2, 1 mM EGTA, 1 mM $MgCl_2$, 0.9 M glycerol, 12.5 mM β-glycerophosphate, 1 mM DTT, 4 μg/ml cytochalasin B, and 7 μg/ml nocodazole), centrosomes were recovered by centrifugation through a 40% sucrose cushion at 50,000 *g* for 30 min at 2°C. The precipitate was suspended in 5 ml of buffer A and centrifuged again through the same sucrose cushion. The precipitate was then extracted with 200 μl of 1 M KCl in buffer B (20 mM Pipes, pH 6.8, 1 mM EGTA, 1 mM $MgCl_2$) on ice for 30 min, followed by centrifugation at 22,000 *g* for 20 min at 2°C. The supernatant, containing pericentriolar material from the egg extracts, was dialyzed against PBS and used as an antigen for mAb production. Hybridomas were produced and screened as described previously (Shiina et al., 1992). We obtained several independent clones producing mAbs including W8C3, which recognized centrosomes of A6 cells on immunofluorescence microscopy.

Cloning of Xenopus and Mouse PCM-1 cDNA

A λZAP II cDNA expression library of *Xenopus* embryo (Stratagene) was screened using mAb W8C3, and several positive clones including clone n1 (2.3-kb cDNA fragment) were obtained. A λgt11 *Xenopus* oocyte cDNA library (Clontech Laboratories, Inc.) was then screened by hybridization with the clone n1 as a probe. Finally, the full-length *Xenopus* PCM-1 cDNA (XPCM-1; clone 23a) was obtained. The predicted open reading frame (ORF) contained 6,093 nucleotides encoding a protein of 2,031 amino acids (aa) with a calculated molecular mass of 228 kD, which showed 56.8% identity to human PCM-1 (hPCM-1) at the amino acid sequence level.

A mouse cDNA library constructed from F9 cells was screened by hybridization with the coding region of XPCM-1 cDNA, and the full-length cDNA for mouse PCM-1 (mPCM-1; clone 16-111) was isolated. The predicted ORF contained 6,075 nucleotides encoding a protein of 2,025 aa with a calculated molecular mass of 229 kD, which showed 57.2% and 87.3% identity to XPCM-1 and hPCM-1 at the amino acid sequence level, respectively.

SDS-PAGE and Immunoblotting

SDS-PAGE (7.5%) was performed according to the method of Laemmli (1970), and proteins were stained with Coomassie brilliant blue. For immunoblotting, proteins were electrophoretically transferred onto polyvinylidene difluoride (PVDF) membranes (Millipore Co.), which were subsequently incubated with the first antibodies. Bound antibodies were detected with biotinylated second antibodies and streptavidin-conjugated alkaline phosphatase (Nycomed Amersham Inc.). Nitroblue tetrazolium and bromochloroindolyl phosphate were used as substrates for detection of alkaline phosphatase.

Generation of Polyclonal Antibodies

The cDNA encoding aa 1,346–2,031 of XPCM-1 (clone n1) or aa 1,299–2,025 of mPCM-1 was subcloned into pGEX-4T-1 or pGEX-5X-3 (Pharmacia Biotech Sverige), respectively, to produce fusion proteins with glutathione S-transferase (GST). These GST fusion proteins were expressed in *E. coli*, purified using glutathione Sepharose 4B columns (Pharmacia Biotech Sverige; Smith and Johnson, 1988), and used as antigens to generate polyclonal antibodies (pAbs) in rabbits. These pAbs were affinity-purified on PVDF membranes with the bands of respective fusion proteins.

Constructs for GFP-XPCM-1 Fusion Proteins

Full-length XPCM-1 (aa 1–2031) and its middle portion (aa 745–1271) were fused with GFP at their COOH termini (GFP-FX and GFP-MX, respectively). To construct the expression vector for GFP-FX, XbaI sites were introduced into both ends of the ORF of XPCM-1 cDNA by site-directed mutagenesis using a Transformer Site-Directed Mutagenesis Kit (CLONTECH Laboratories, Inc.) with primers 5′-CTGCAAACCATGTCTAGAGGAGGAGGTCC-3′ and 5′-GCCATCCACCCTG-

CATCTAGAGAAACTGACAAACAAG-3′. The XbaI–XbaI fragment was subcloned into the NheI site of the pQB125 GFP expression vector (Quantum Biotechnologies, Inc.). To construct the expression vector for GFP-MX, MluI sites and KpnI sites were introduced into both ends of the regions encoding aa 1–744 and aa 1272–2031, respectively, in the GFP-FX expression vector by site-directed mutagenesis with primers 5′-CGCGCAAGAAATGACGCGTGGAGGAGGTCCAC-3′/5′-CCAAATAACACGCGTCCAATGTGTC-3′ and 5′-CTTTCAGCAGGTGGTACCTCAGCCAAGCTGG-3′/5′-GCCATCCACCCTGGTACCAGCAAAGGAGAAGAAC-3′. This plasmid was digested with MluI, followed by self-ligation, and then digested with KpnI, followed by self-ligation, to generate the GFP-MX expression vector. All expression vectors were confirmed by sequencing.

Observation of GFP Fusion Proteins in Live Cells

A6 cells were transfected with the GFP-FX or GFP-MX expression vector, and stable transfectants were obtained (GFX-A6 and GMX-A6 cells, respectively) as described previously (Shiina and Tsukita, 1999). These transfectants were observed using a DeltaVision microscope (Applied Precision, Inc.) equipped with an Olympus IX70 microscope and a cooled charge-coupled device (CCD) system. Each image was acquired with 1-s exposure of the CCD camera.

In Vitro Motility Assay

Centrosomes were isolated from A6 cells, and rhodamine-labeled tubulin was obtained from bovine brain as described previously (Mitchison and Kirschner, 1984; Bornens et al., 1987; Hyman et al., 1991). GMX-A6 cells were collected and homogenized in PEM35 buffer (35 mM Pipes, pH 7.1, 0.5 mM EGTA, 0.5 mM $MgCl_2$) containing 0.2 M sucrose, 1 mM DTT, 0.4 μg/ml nocodazole, 10 μg/ml pepstatin, 10 μg/ml leupeptin, and 1% aprotinin, and were then layered onto a 0.3–1.2 M linear sucrose density gradient of PEM35 buffer. After centrifugation at 20,000 *g* for 30 min, the fraction enriched in GFP-tagged centriolar satellites was collected and centrifuged at 100,000 *g* for 1 h. The pellet was resuspended in the supernatant (200,000 *g* for 10 min) of *Xenopus* egg extract, and 1/20 vol of isolated centrosomes and 1/80 vol of rhodamine-labeled purified porcine brain tubulin were added on ice. The mixture was spread onto glass coverslips, warmed to 22°C, and then observed with the DeltaVision microscope. In some experiments, AMP-PNP (Sigma Chemical Co.), sodium orthovanadate (Wako Pure Chemicals), or mouse antidynein intermediate chain mAb (m70.1; Sigma Chemical Co.) was added to the mixture on ice for 20 min, followed by further incubation for 10 min at 22°C before observation.

Induction of Ciliogenesis in Mouse Nasal Respiratory Epithelia

Nasal respiratory epithelia of C57/B6 mice were irritated with 1% aqueous $ZnSO_4$ solution as described previously (Matulionis, 1975). The $ZnSO_4$ treatment induces necrosis of ciliated cells in the C57/B6 strain of mice. As a result, the entire layer of epithelium is sloughed off so that the cilia-bearing cells are reformed with concomitant centriologenesis and ciliogenesis (Matulionis, 1975). In brief, a drop of 1% $ZnSO_4$ solution was applied to the orifice of external nares to be inhaled by the mouse. This procedure was repeated until at least three drops had been aspirated into the nasal chambers. The mice were treated in this manner three times at intervals of 30 min. Control mice were exposed to distilled water. Mice were killed 4 d after treatment, and 1% paraformaldehyde in 100 mM phosphate buffer (pH 7.4) was immediately injected into the nasal cavities. Nasal epithelial tissues were quickly removed from the mice, treated with the same fixative for 30 min on ice, washed with PBS three times, and processed for immunofluorescence and immunoelectron microscopy.

Immunofluorescence Microscopy

Xenopus A6 cells cultured on glass coverslips were fixed with methanol for 5 min at −20°C and processed for immunofluorescence microscopy as described previously (Shiina et al., 1992). Mouse anti–α-tubulin mAb (DM1A; Sigma Chemical Co.) and mouse anti–γ-tubulin mAb (GTU-88; Sigma Chemical Co.) were used as the primary antibodies, and Cy3-conjugated goat anti–rabbit IgG antibody and Cy2-conjugated donkey anti–mouse IgG antibody (Nycomed Amersham, Inc.) were used as secondary antibodies.

Small pieces of mouse nasal respiratory epithelia fixed in 1% paraformaldehyde were infused with 2.3 M sucrose containing 20% polyvinylpyrrolidone at 4°C overnight, rapidly frozen in liquid nitrogen, then cut into cryosections ~0.5-μm thick at −110°C. They were then mounted on poly-L-lysine coated glass coverslips, treated with 0.12% glycine in PBS for 30 min, and processed for immunofluorescence microscopy as described previously (Tokuyasu, 1980; Fujimoto et al., 1992). Specimens were observed using a fluorescence microscope (Axiophot photomicroscope; Carl Zeiss, Inc.), or an MRC 1024 laser-scanning confocal microscope (Bio-Rad Laboratories) equipped with a Zeiss Axioplan 2 photomicroscope. Images gained by laser-scanning confocal microscopy were integrated from the optical sections recorded at intervals of 0.2 μm.

Electron Microscopy

Conventional EM for A6 cells and nasal respiratory epithelium of mouse was performed as described previously (Yonemura et al., 1995). For immunoelectron microscopy of A6 cells, cells cultured on glass coverslips were fixed with 0.25% glutaraldehyde in PEM80 buffer (80 mM Pipes, pH 6.8, 1 mM EGTA, and 1 mM $MgCl_2$) containing 1% Triton X-100 for 10 min at room temperature, and processed for immunoelectron microscopy according to the method described previously (Wittmann et al., 1998). For immunoelectron microscopy of in vitro reconstituted asters, samples were prepared as follows. The fraction enriched in centriolar satellites was prepared from nontransfected A6 cells as described above. This fraction was resuspended in the supernatant of *Xenopus* egg extract, and then 1/10 vol of isolated centrosomes was added. The mixture was incubated at room temperature for 20 min and processed for immunoelectron microscopy as described previously (Wittmann et al., 1998). For preembedding immunoelectron microscopy of mouse nasal epithelia, samples were treated with PEM80 buffer containing 0.5% Triton X-100 for 6 min, fixed with 0.25% glutaraldehyde in PEM80 buffer containing 1% Triton X-100 for 10 min, and processed as described previously (Wittmann et al., 1998). For postembedding immunoelectron microscopy of mouse nasal epithelia, small pieces fixed in 1% paraformaldehyde were infused with 2.3 M sucrose containing 20% polyvinylpyrrolidone at 4°C overnight and rapidly frozen in liquid nitrogen. Ultrathin cryosections were cut and processed for immunolabeling, according to the method developed by Tokuyasu (1980; Fujimoto et al., 1992). Goat anti–rabbit IgG coupled to 10-nm gold (Nycomed Amersham Inc.) was used as a secondary antibody. Samples were examined with an electron microscope (JEM 1010; JEOL) at an accelerating voltage of 100 kV.

Online Supplemental Material

A movie file corresponding to Fig. 4 a is available online (http://www.jcb.org/cgi/content/147/5/969/F4/DC1). Time-lapse images collected using DeltaVision were processed with Adobe Photoshop software and converted to a QuickTime movie (JPEG compression) with Adobe Premiere Software. This movie contains the time-lapse images from the first to the last panel in the corresponding figures. Images were recorded for 3 min at 5–6 s intervals.

Results

Localization of PCM-1 in Centriolar Satellites

To analyze the molecular components of centrosomes, we raised mAbs against pericentriolar material isolated from *Xenopus* egg extracts. Since one of these mAbs, W8C3, stained centrosomes of cultured *Xenopus* epithelial A6 cells, we isolated a full-length cDNA encoding its antigen by screening a *Xenopus* embryo λZAP II cDNA expression library. DNA sequencing revealed that its product encoded a protein of 2,031 aa with significant similarity to human PCM-1 (hPCM-1; 56.8% identity at the amino acid sequence level), indicating that W8C3 recognized a *Xenopus* homologue of PCM-1 (XPCM-1; sequence data are available from GenBank/EMBL/DDBJ under accession number AB025414). As this mAb showed some cross-reactivity with α-tubulin, we then raised a pAb against re-

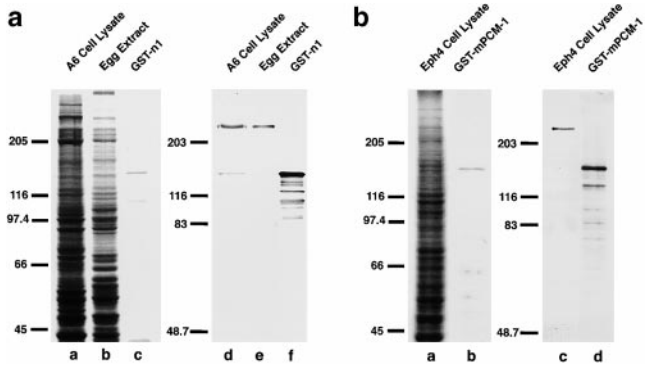

Figure 1. Specificity of pAbs. a, Rabbit anti–*Xenopus* PCM-1 (XPCM-1) pAb. Total cell lysate of cultured *Xenopus* A6 cells (A6 Cell Lysate) and *Xenopus* egg extract (Egg Extract), and purified GST fusion protein with the COOH-terminal portion of XPCM-1 produced in *E. coli* (GST-n1) were separated by SDS-PAGE (a–c; CBB staining), followed by immunoblotting with anti–XPCM-1 pAb (d–f). This affinity-purified pAb specifically recognized ~230 kD XPCM-1 in d and e, as well as GST fusion protein in f. b, Rabbit anti–mouse PCM-1 (mPCM-1) pAb. Total cell lysate of cultured mouse Eph4 cells (Eph4 Cell Lysate) and purified GST fusion protein with the COOH-terminal portion of mPCM-1 produced in *E. coli* (GST-mPCM-1) were separated by SDS-PAGE (a and b; CBB staining), followed by immunoblotting with anti–mPCM-1 pAb (c and d). This affinity-purified pAb specifically recognized ~230 kD mPCM-1 in c, as well as GST fusion protein in d.

combinant XPCM-1 produced in *E. coli*. As shown on immunoblots, this pAb specifically recognized a 230-kD band in A6 cell lysates, as well as *Xenopus* egg extracts (Fig. 1 a). Judging from the molecular mass of human PCM-1 (~230 kD) and from the reactivity of this pAb with recombinant *Xenopus* PCM-1, we concluded that this pAb specifically recognized XPCM-1.

Next, to examine the subcellular localization of XPCM-1 by immunofluorescence microscopy, cultured A6 cells were doubly stained with the anti–XPCM-1 pAb and anti–γ-tubulin mAb (Fig. 2, a–c). The γ-tubulin signal was exclusively detected in centrosomes, whereas XPCM-1 was concentrated on and/or around γ-tubulin–positive centrosomes in large amounts, and was also scattered in the cytoplasm in a punctate manner in small amounts. In metaphase, its concentration around centrosomes became obscure as previously described in HeLa cells (Balczon et al., 1994; data not shown). Interestingly, when these XPCM-1–positive granular structures were examined in Triton X-100–treated A6 cells by immunoelectron microscopy, anti–XPCM-1 pAb specifically labeled electron-dense spherical granules 80–90 nm in diameter located around centrosomes (Fig. 2 d). Some of these granules appeared to be associated with MTs. Conventional EM of A6 cells also identified similar electron-dense granules gathering around centrosomes, which were not surrounded by membranes (Fig. 2 e). Judging from their morphological characteristics, we concluded that these granules were identical to the previously described structures designated as centriolar satellites (Bernhard and De Harven, 1960; de-Thé, 1964; Berns et al., 1977). As shown in Fig. 2, d and e, pale granules with a similar diameter were also observed around centrioles, but these granules were not labeled with anti–XPCM-1 pAb.

MT-dependent Localization of Centriolar Satellites around Centrosomes

Occasional association of PCM-1–containing granules with MTs led us to examine whether MTs are required to determine their pericentriolar localization, i.e., whether their localization is affected by the MT-depolymerizing agent nocodazole. When A6 cells were treated with 0.4 μg/ml nocodazole for 2 h, followed by immunostaining doubly with anti–XPCM-1 pAb and anti–α-tubulin mAb, most of the centriolar satellites (XPCM-1–positive dots) were released from centrosomes and were scattered into the cytoplasm with concomitant destruction of MT networks (data not shown). When the nocodazole was washed out from these cells, within 9 min MTs began to elongate from centrosomes and concomitantly centriolar satellites increased in number around centrosomes. At 12 min after washing out of nocodazole, most of the centriolar satellites were reconcentrated around centrosomes, from which a well developed MT network was reorganized. In contrast, the actin-depolymerizing agent cytochalasin B (1–10 μg/ml) did not affect the localization of centriolar satellites (data not shown). These findings indicated that centriolar satellites are concentrated around centrosomes in a manner dependent on the MT network.

Behavior of Centriolar Satellites in Living Cells

To examine the interaction between centriolar satellites and MTs in more detail, we observed the behavior of centriolar satellites in live A6 cells. We constructed cDNAs encoding fusion proteins of GFP with the full-length (aa 1–2031) or middle portion (aa 745–1271) of XPCM-1 (designated as GFP-FX and GFP-MX, respectively), and introduced them into A6 cells to obtain stable transfectants (designated as GFX-A6 and GMX-A6 cells, respectively). In both transfectants, GFP-derived fluorescence was detected as small granules in large numbers around centrosomes and in small numbers scattered in the cytoplasm (GFX-A6, data not shown; GMX-A6, see Fig. 3 a). Since the anti–XPCM-1 pAb described above was raised against the COOH-terminal region of XPCM-1 (aa 1346–2031), this pAb recognized endogenous XPCM-1, but not GFP-MX. However, when GMX-A6 cells were stained with this pAb, the GFP fluorescence signal overlapped the region of staining with the anti–XPCM-1 pAb (Fig. 3, a–c). These findings indicated that each centriolar satellite contains multiple XPCM-1 molecules, and that the middle portion of the XPCM-1 is sufficient for incorporation into centriolar satellites.

Since GMX-A6 cells gave stronger GFP fluorescence signals than GFX-A6 cells, we used the former transfectants to examine the movement of centriolar satellites in live cells. As shown in Fig. 3 a, in these cells, individual granules were not resolved around centrosomes, but were readily detected in the cytoplasm. These single granules moved linearly at maximum rates of ~0.7–0.8 μm/s. They frequently changed their velocity, as well as direction of movement, and repeatedly cycled through moving and sta-

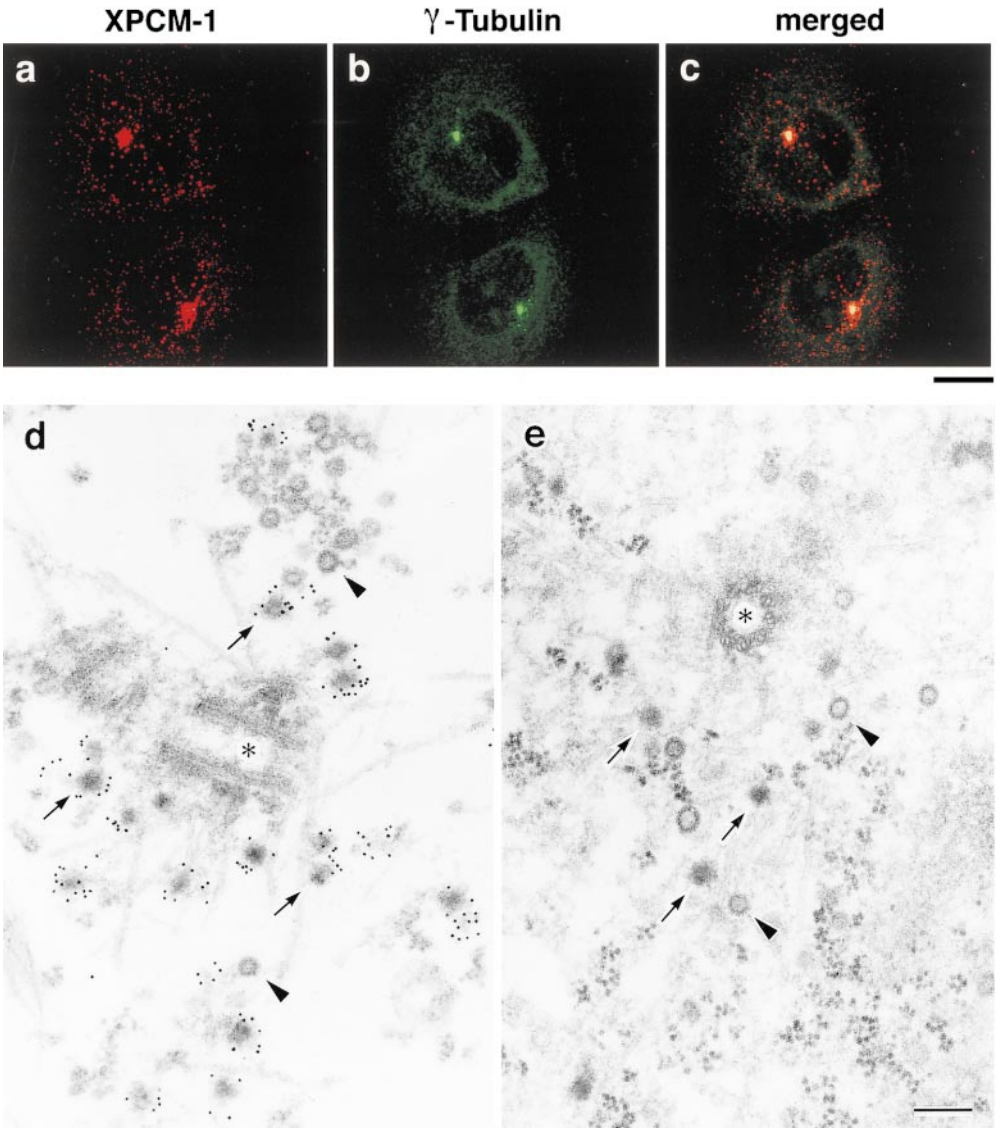

Figure 2. Subcellular localization of XPCM-1 in A6 cells. a–c, Double immunofluorescence staining of A6 cells with anti–XPCM-1 pAb (a) and anti–γ-tubulin mAb (b). The merged image (c) revealed that most of the XPCM-1–positive granular structures were concentrated on and/or around γ-tubulin–positive centrosomes. Small numbers of XPCM-1–positive granular structures were observed scattered in the cytoplasm. Bar, 10 μm. d, Localization of XPCM-1 at centriolar satellites. When A6 cells were treated with Triton X-100 and labeled with anti–XPCM-1 pAb, numerous electron dense granules (arrows) around the centrosome (asterisk) were specifically labeled at the electron microscopic level. Some granules appeared to be associated with MTs. Note that pale granules (arrowheads) with similar diameter were not labeled. e, Ultrastructure of centrosomes of A6 cells in situ. A6 cells were processed for ultrathin EM without Triton X-100 treatment. Note the so-called centriolar satellites (arrows) and pale granules (arrowheads) around the centrosome (asterisk). Bar, 200 nm.

tionary states. In cultured GMX-A6 cells, single centriolar satellites in the cytoplasm appeared to move not only toward centrosomes, but also toward the cell periphery (Fig. 3, d–g). Nocodazole (0.4 μg/ml), but not cytochalasin B (1–10 μg/ml), affected these directional movements of centriolar satellites (data not shown).

MT-dependent Movement of Centriolar Satellites In Vitro

Observations in live cells suggested that centriolar satellites moved along MTs. Therefore, we next examined the interaction of MTs and centriolar satellites in vitro. GFP-tagged centriolar satellites were partially purified from GMX-A6 cells. Asters were reconstituted in vitro from centrosomes isolated from A6 cells, rhodamine-labeled tubulin purified from porcine brain, and 200,000 *g* supernatant of *Xenopus* egg extracts. Then, the isolated centriolar satellites were mixed with reconstituted asters in the presence of ATP. As shown in Fig. 4 a and the movie, at the beginning of observation by fluorescence microscopy, numerous GFP-tagged centriolar satellites were already gathered in the center of reconstituted asters, but close inspection revealed single granules moving along MTs. These granules moved toward the minus end of MTs, i.e., toward the centrosomes. No granules were observed moving toward the plus end of MTs. Similarly to the in vivo observations, these granules repeatedly alternated between the stationary and moving states. Their maximum velocity was 0.7 μm/s, which was compatible to that in vivo. As shown in Fig. 4 a, these granules had frequent changes of MTs.

We then examined the centriolar satellites gathered around centrosomes in the in vitro reconstituted system by immunoelectron microscopy. Numerous electron-dense nonmembranous granules, ~80–90 nm in diameter, were observed around centrosomes, and these were labeled with anti–XPCM-1 pAb (Fig. 4 b). Of course, no granules were observed in asters that were reconstituted in the absence of isolated centriolar satellites (data not shown). At the periphery of asters, anti–XPCM-1 pAb-labeled elec-

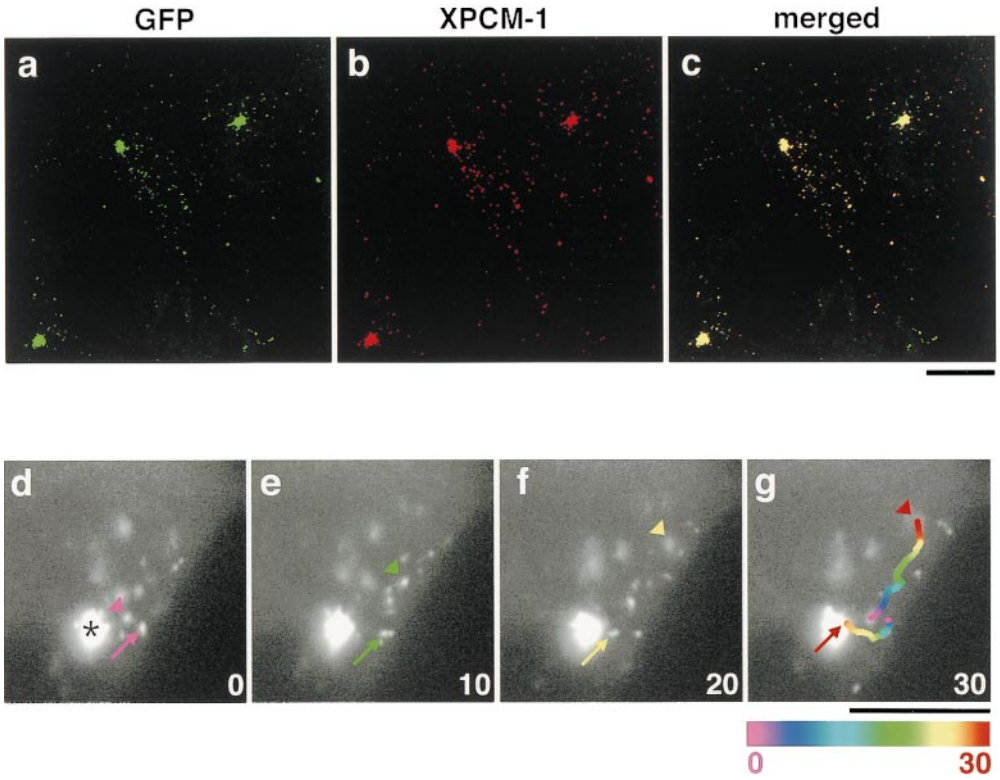

Figure 3. Movement of GFP-tagged centriolar satellites in live A6 cells. a–c, GMX-A6 cells, A6 transfectants stably expressing GFP fusion protein with the middle portion of XPCM-1 (GFP-MX), were stained red with anti–XPCM-1 pAb. Since this pAb did not recognize GFP-MX, it represented the localization of endogenous XPCM-1 (b). Most of the green fluorescence from expressed GFP-MX (a) was colocalized with endogenous XPCM-1 (b and c). d–g, Image series of GMX-A6 cells showing the movement of GFP-tagged centriolar satellites. Numbers at the bottom right indicate the time lapse in seconds. Arrows show the movement of granules toward the centrosome (asterisk), and arrowheads indicate granules moving toward the cell periphery. When the granules moved quickly during 1-s exposure of the CCD camera, they appeared tube-like in shape (arrow in f). In g, the paths of movement of two granules during 30 s were traced, which were represented in 2-s intervals beginning with the coolest colors (purple) and proceeding to the hottest colors (red). Bars, 10 μm.

tron-dense granules were occasionally seen to be associated with MTs, which may have been on the way to centrosomes (data not shown).

To identify the motor protein responsible for this in vitro movement of GFP-tagged centriolar satellites, we examined the effects of some inhibitors of motor proteins (Fig. 5). At 10 μM, vanadate abolished the accumulation of centriolar satellites around centrosomes. This finding suggested that dynein was involved, since dynein, but not kinesin, is inhibited by low concentrations of vanadate (10–20 μM; Schroer and Sheetz, 1989). AMP-PNP did not affect centriolar satellite accumulation at a concentration of 100 μM, whereas at higher concentrations, such as 2 mM, AMP-PNP showed complete suppression. This again favored the notion that dynein is responsible for the centriolar satellite movement, since 100 μM AMP-PNP inhibits kinesin, but not dynein (2 mM AMP-PNP inhibits both; Schroer and Sheetz, 1989). In good agreement with these observations, antidynein intermediate chain mAb (m70.1; 60 μg/ml) completely abolished the accumulation of GFP-tagged centriolar satellites around centrosomes, while control IgG had no effect.

PCM-1 in Fibrous Granules Associated with Ciliogenesis

The pericentriolar localization of PCM-1–containing centriolar satellites and their disappearance in mitotic cells (Balczon et al., 1994) suggested some association of these granules with the replication cycle of centrioles. During experimentally induced ciliogenesis, numerous centrioles (ciliary basal bodies) were known to be replicated in a synchronized manner within individual cells, providing a good system to examine centriolar replication (Anderson and Brenner, 1971). We then examined the expression and behavior of PCM-1 in mouse nasal respiratory epithelium, since ciliogenesis can be induced simply by irritation with 1% aqueous $ZnSO_4$ (Matulionis, 1975).

First, full-length cDNA encoding mouse PCM-1 (mPCM-1) was isolated. Its product encoded a protein of 2,025 aa with significant similarity to hPCM-1 and XPCM-1 (87.3% and 57.2% identity at the amino acid sequence level, respectively; the sequence data are available from GenBank/EMBL/DDBJ under accession number AB029291). Then, using recombinant mPCM-1 produced in *E. coli* as an antigen, a pAb was generated. This pAb specifically recognized an ~230-kD band in the total lysate of mouse Eph4 cells on immunoblots (Fig. 1 b) and exclusively labeled centriolar satellites of Eph4 cells at the electron microscopic level (data not shown). Interestingly, when cryosections of mouse nasal respiratory ciliated epithelium were immunofluorescently stained with this pAb, the mPCM-1 signal was specifically detected at their apical cytoplasm in a granular pattern (Fig. 6, a and c). Four days after irritation of the nasal epithelia with 1% aqueous $ZnSO_4$ in situ, cilia were completely removed from their apical surface (Fig. 6 d) and, interestingly, the mPCM-1 signal was markedly elevated at the apical cytoplasm (Fig.

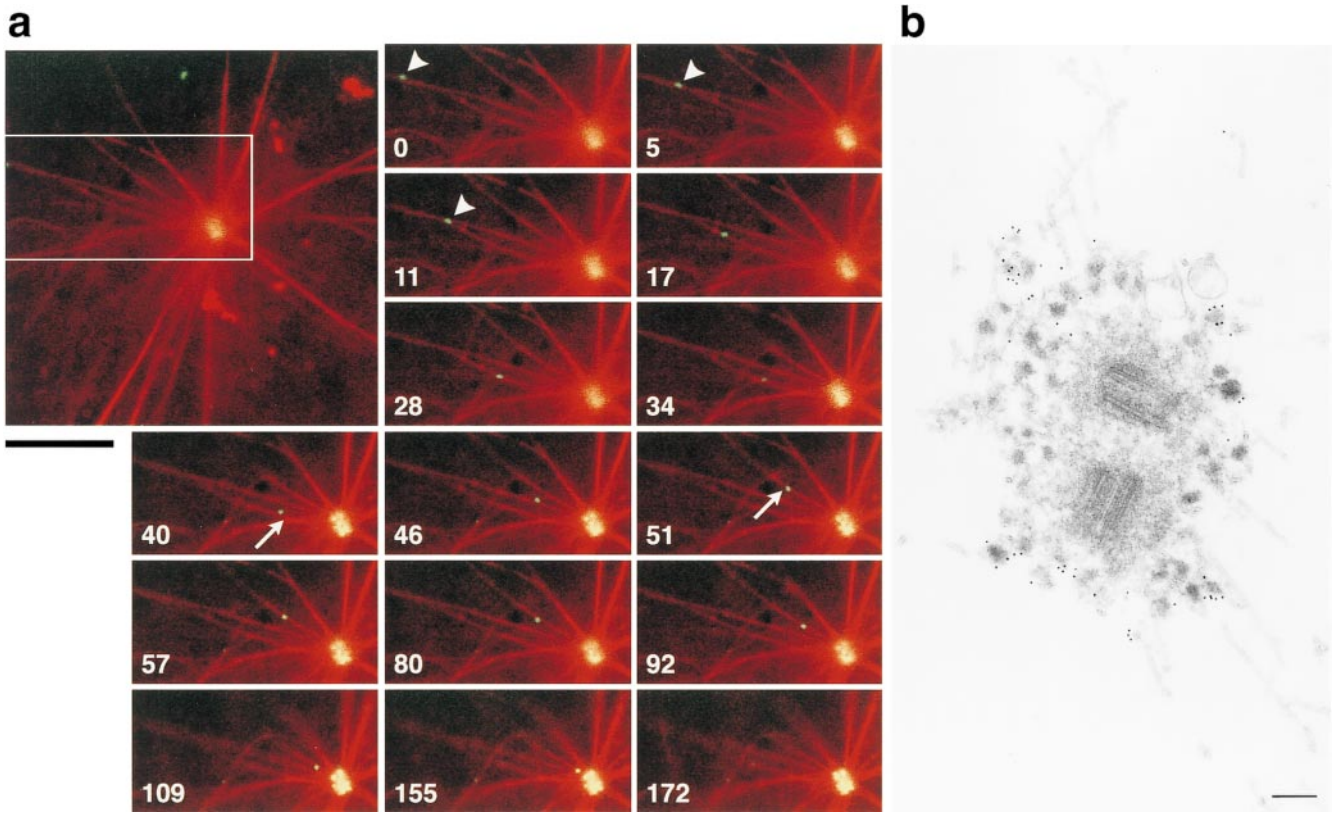

Figure 4. In vitro motility of GFP-tagged centriolar satellites. a, Time-lapse observation of the movement of a centriolar satellite (green) in a reconstituted aster (red). The boxed area in the large panel is magnified in the small panels. Numbers at the bottom left in the small panels indicate the time lapse in seconds. GFP-tagged centriolar satellite (arrowheads) moved along a MT toward centrosomes where other granules had already accumulated. On the way to the centrosome, this granule changed MTs (arrows), and finally reached the centrosome. Bar, 10 μm. A QuickTime movie is available at http://www.jcb.org/cgi/content/147/5/969/F4/DC1. b, Immunoelectron microscopy of centriolar satellites accumulating around centrosomes in the in vitro reconstituted asters. Electron-dense granular structures, ~80–90 nm in diameter, which were specifically labeled with anti–XPCM-1 pAb (10-nm gold particles), were accumulated around fibrous materials of centrosomes. These XPCM-1–containing granules were not delineated by membranes. Bar, 200 nm.

6, b and d). Then, we examined the $ZnSO_4$-induced morphological changes of these ciliated epithelia at the electron microscopic level.

Conventional ultrathin EM revealed that in nontreated ciliated cells, electron-dense granules ~100 nm in diameter were scattered beneath the layer of basal bodies of cilia (Fig. 7 a). Curiously, these granules were morphologically indistinguishable from centriolar satellites. As shown in Fig. 7, b and c, both preembedding and postembedding immunolabeling revealed that these granules were exclusively labeled with anti–mPCM-1 pAb. When cilia were removed from these respiratory epithelia by $ZnSO_4$ treatment, these granules appeared to increase in number and aggregated extensively (Fig. 7 d). In previous reports, these granules were called fibrous granules and were thought to be absent in nonciliogenic cells (Sorokin, 1968; Steinman, 1968; Anderson and Brenner, 1971; Dirksen, 1991), but this was not likely. This will be confirmed by the subsequent immunoelectron microscopy. In or close to the aggregation of these granules called fibrogranular area, so-called deuterosomes with multiple replicating procentrioles appeared (Fig. 7 d). These morphological characteristics indicated that synchronized multiple centriolar replication and subsequent ciliogenesis were induced in these cells. Preembedding immunoelectron microscopy revealed that these aggregated fibrous granules, but not deuterosomes, were heavily labeled with anti–mPCM-1 pAb (Fig. 7 e). Since deuterosomes were very large electron-dense structures, it was possible that antibodies cannot access the antigen within deuterosomes. However, postembedding immunolabeling did not detect mPCM-1 within deuterosomes, excluding this possibility (Fig. 7 f). Taken together, we concluded that so-called fibrous granules, which had been intensively examined from the viewpoint of centriolar replication, may be identical to PCM-1–containing centriolar satellites.

Discussion

Various types of membranous and nonmembranous organelles have been described in eukaryotic cells, and their structures and functions have been analyzed in detail. However, there are likely to be many organelles that have not been identified or characterized. The centriolar satellite, electron-dense spherical granules ~70–100 nm in diameter, occurring around centrioles in most types of cells,

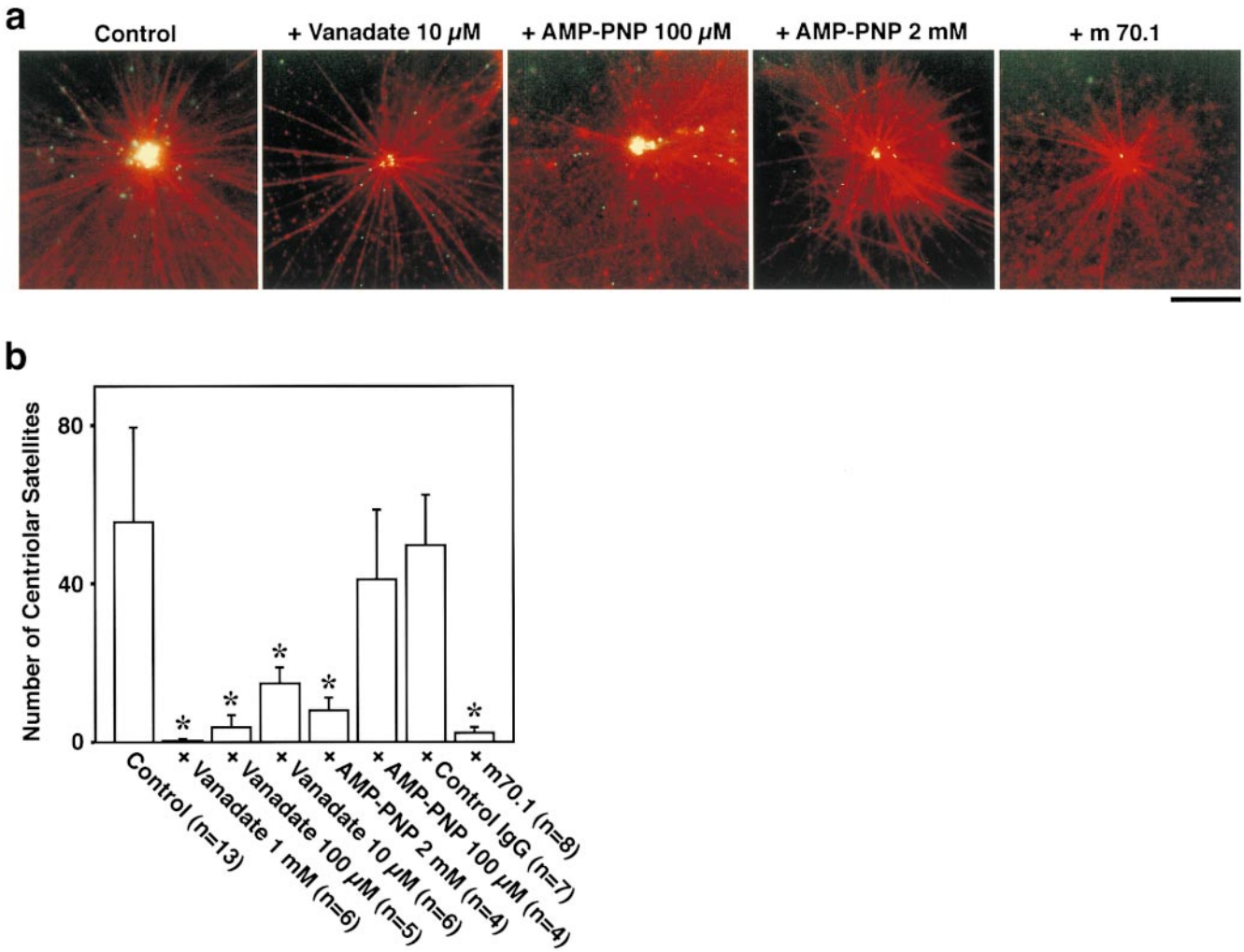

Figure 5. Inhibition of the accumulation of GFP-tagged centriolar satellites around centrosomes in vitro. A reconstituted aster (red) was incubated with GFP-tagged centriolar satellites (green) under the same condition as Fig. 4 a. Without additional reagents, numerous granules were accumulated around the centrosome during 10-min incubation (Control). AMP-PNP at 2 mM, but not 100 μM, significantly suppressed the accumulation of granules. 10 μM vanadate, as well as antidynein intermediate chain mAb (m70.1), also completely suppressed the accumulation. When the accumulation was suppressed, the movement of individual granules itself was always affected. Bar, 10 μm. b, The number of centriolar satellites, which were accumulated around centrosomes during 10-min incubation, were counted per individual centrosomes. Asterisks, *F*-test showed significant inhibition ($P < 0.001$).

is one such uncharacterized type of nonmembranous organelle. In this study, we identified PCM-1 as the first component of the centriolar satellite in *Xenopus* A6 and mouse Eph4 cells. Transfection experiments of a truncated form of XPCM-1 showed that multiple XPCM-1 molecules were incorporated into each granule, and our preliminary experiments showed that these molecules bind directly to each other to form dimers or oligomers, suggesting that PCM-1 is a kind of scaffold protein constituting the centriolar satellites. Fibrous granules also constitute an uncharacterized type of nonmembranous organelle. These granules were thought to appear in ciliated cells only during ciliologenesis, but we found that they were also distributed close to ciliary basal bodies in nonciliogenic phase. These granules also had the appearance of electron-dense spherical granules ~80–90 nm in diameter, and were indistinguishable morphologically from the centriolar satellites, although this resemblance has not been described previously. Interestingly, we found that these granules also contained PCM-1. Therefore, we propose here that centriolar satellites and fibrous granules can be regarded as the same novel nonmembranous organelles, defined by their specific component, PCM-1.

One of the most characteristic features of centriolar satellites (so probably also fibrous granules) is their ability to move along MTs; they moved along MTs toward their minus ends, i.e., toward centrosomes, in reconstituted asters in vitro in the presence of ATP. The effects of AMP-PNP, vanadate, and antidynein mAb suggested that dynein, but not kinesin, was involved in their movement. In good agreement, Balczon et al. (1999) recently reported that PCM-1 was coprecipitated with MTs from CHO cell extracts, and that immunodepletion with antidynein antibody, not antikinesin antibody, from CHO extracts significantly decreased the amount of coprecipitated PCM-1. Furthermore, PCM-1 was shown to directly bind to Hun-

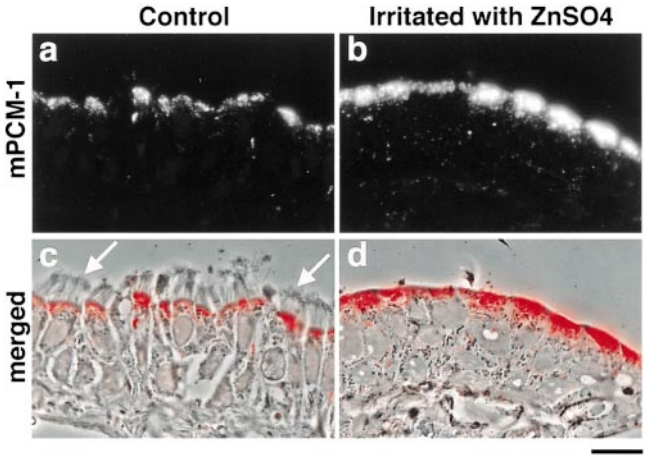

Figure 6. Subcellular distribution of mouse PCM-1 (mPCM-1) in mouse nasal respiratory epithelium. When cryosections ~0.5-μm thick of ciliated epithelium were immunofluorescently stained with anti–mPCM-1 pAb (a, red in c), mPCM-1 signal was detected at the apical cytoplasm of epithelial cells (c; a composite with the phase-contrast image). Arrows, cilia. At four days after irritation of the nasal epithelia with 1% aqueous $ZnSO_4$ in situ, cilia were completely removed from their apical surface, and the PCM-1 signal at the apical cytoplasm was markedly elevated (b, red in d). d, a composite with the phase-contrast image. Bar, 10 μm.

tingtin-associated protein 1 (HAP1) by yeast two hybrid analyses (Engelender et al., 1997). Since HAP1 bound to the $p150^{Glued}$ subunit of dynactin complex (Engelender et al., 1997), HAP1 may function as a cross-linker between PCM-1, i.e., the centriolar satellites (and also fibrous granules), and the dynein/dynactin complexes.

The dynein-dependent, minus end-directed movement can explain the pericentriolar localization of centriolar satellites. In live A6 cells, GFP-tagged centriolar satellites moved not only toward centrosomes, but also toward the cell periphery. It is clear that the centripetal movement dominates as a whole, since centriolar satellites accumulated around centrosomes in live cells, but it remains unclear whether centriolar satellites also bear plus end-directed motors such as kinesins, or some fraction of MTs of A6 cells do not originate from centrosomes and these MTs are responsible for the centrifugal movement of centriolar satellites. The localization of fibrous granules close to ciliary basal bodies in ciliated epithelial cells in the nonciliogenic phase could also be explained in the same way. In simple epithelial cells, most of the minus ends of MTs are not anchored at the centrosome, but are scattered throughout their apical regions with MTs running parallel along the apico-basal axis (Bacallao et al., 1989; Mogensen et al., 1989). Therefore, if the fibrous granules are also associated with dynein, they would accumulate at the apical regions of epithelial cells.

The physiological functions of the centriolar satellites remain unclear. As shown in this study, however, their resemblance to the fibrous granules not only morphologically, but also in their molecular composition, suggested that they may play some roles in centriolar replication. Fibrous granules were reported to be associated with the replication of basal bodies (Sorokin, 1968; Anderson and Brenner, 1971). In good agreement, the level of PCM-1 was markedly elevated when ciliogenesis was induced in nasal epithelial cells (Fig. 6, b and d). In addition to fibrous granules, larger electron-dense spherical structures called deuterosomes also emerged during centriolar replication in ciliogenic cells, from which multiple procentrioles grew (Sorokin, 1968), and previous electron microscopic observations suggested that fibrous granules were fused to form deuterosomes (Sorokin, 1968; Anderson and Brenner, 1971). However, this was not likely since PCM-1 was detected in fibrous granules, but not in deuterosomes (Fig. 7, e and f). The experimentally induced ciliogenesis examined in this study will be an advantageous system to further analyze the relationship between PCM-1–containing granules and centriolar replication in future studies.

Previous studies on PCM-1 itself also suggested its possible association with centriolar replication. It is widely accepted that centriolar replication begins near the G1/S boundary, continues through S phase, and is completed during G2 phase (Robbins et al., 1968; Brinkley, 1985; Vandré and Borisy, 1989). In good agreement, PCM-1 at centrosomes is released into the cytoplasm on the entry to M phase, and on the entry to interphase this molecule is reconcentrated at centrosomes (Rattner, 1992; Balczon et al., 1994). PCM-1 mRNA levels increase through G1 and S phases, and became undetectable during G2 and M phases in CHO cells (Balczon et al., 1995). Interestingly, PCM-1 mRNA levels remained elevated during multiple rounds of centrosome replication in CHO cells arrested at the G1/S boundary by hydroxyurea with a concomitant increase in number of centriolar satellites (see Figure 4 in Balczon et al., 1995).

On the other hand, fibrous granules were also suggested to function as axonemal precursors (Steinman, 1968). Recent studies using *Chlamydomonas* identified intraflagellar transport (IFT) particles as large preassembled precursors for various axonemal structures in cytoplasm that were concentrated around centrioles (Cole et al., 1998; Rosenbaum et al., 1999). However, it is not likely that fibrous granules are the counterparts of IFT particles; IFT particles are lollipop-shaped electron-dense granules, ~14–19 nm in diameter (see Figure 3 in Kozminski et al., 1993), which is much smaller than fibrous granules. IFT particles were detected within flagella, while fibrous granules or PCM-1 was not observed within cilia. Furthermore, PCM-1 immunofluorescence was abundant in the apical cytoplasm of nonciliated epithelial cells, such as intestinal and gastric epithelial cells (Kubo, A., A. Yuba-Kubo, S. Tsukita, and N. Shiina, unpublished data). These findings are against the notion that fibrous granules function as axonemal precursors. Further identification of other components of fibrous granules/centriolar satellites will answer these questions more clearly.

In this study, we identified pericentriolar satellites and fibrous granules as PCM-1–containing novel nonmembranous organelles, which were accumulated around centrosomes and ciliary basal bodies, respectively, through their minus end-directed movement along MTs. These findings then suggested the possible association of these PCM-1–containing organelles with centriolar replication. Further detailed analyses of these organelles, as well as PCM-1 molecules, will lead to a better understanding of the molecular mechanism of centriologenesis in general.

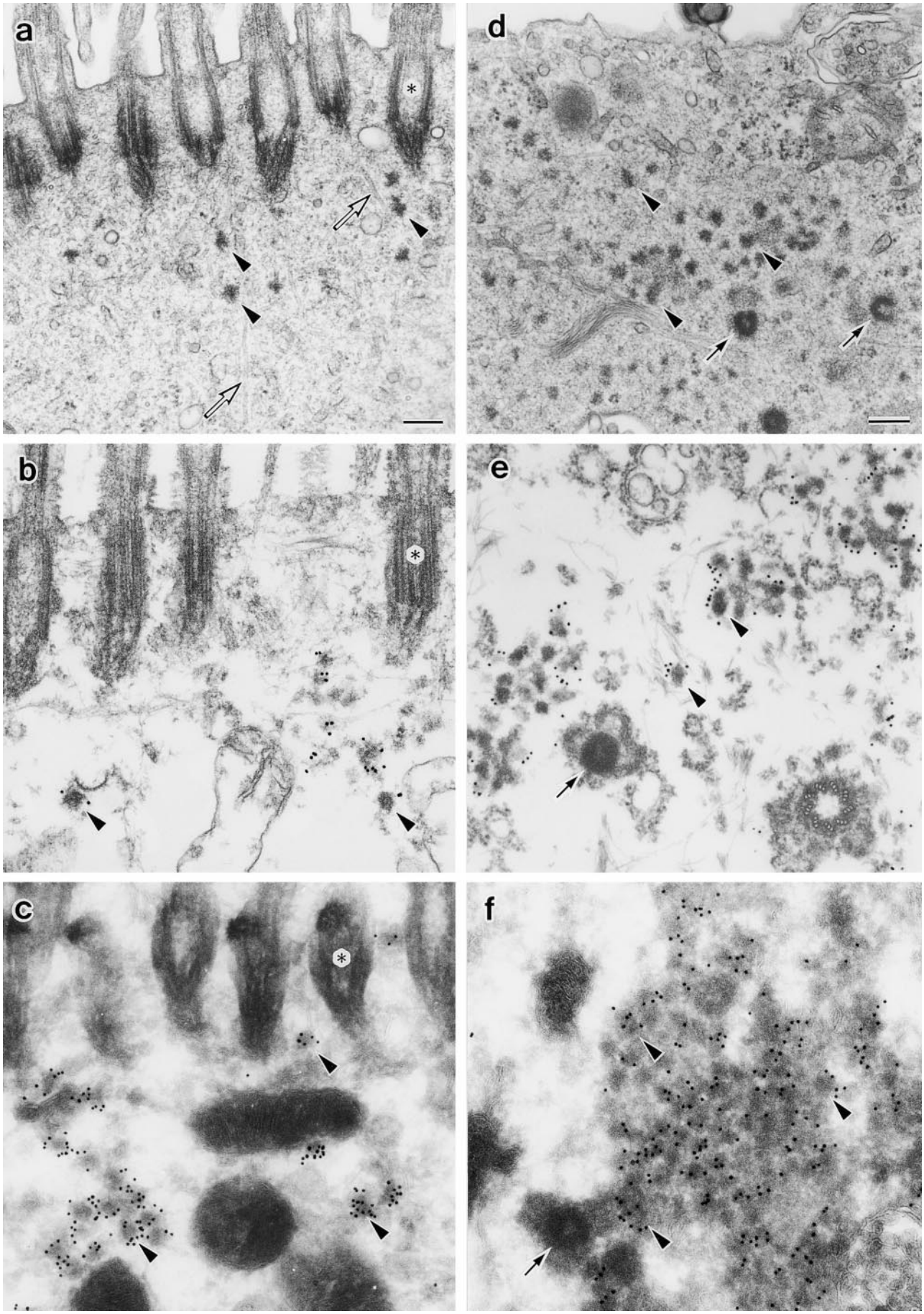

Figure 7.

We thank Y. Matsumoto and E. Nishida (Kyoto University) for their collaboration in XPCM-1 cDNA screening. Thanks are also due to Ms. K. Janjin Matsubara for technical support in EM, and Drs. Y. Mimori-Kiyosue and S. Yonemura for technical advice and helpful discussions.

Submitted: 29 July 1999
Revised: 28 September 1999
Accepted: 14 October 1999

References

Anderson, R.G.W., and R.M. Brenner. 1971. The formation of basal bodies (centrioles) in the rhesus monkey oviduct. *J. Cell Biol.* 50:10–34.

Bacallao, R., C. Antony, C. Dotti, E. Karsenti, E.H. Stelzer, and K. Simons. 1989. The subcellular organization of Madin-Darby canine kidney cells during the formation of a polarized epithelium. *J. Cell Biol.* 109:2817–2832.

Balczon, R., L. Bao, and W.E. Zimmer. 1994. PCM-1, A 228-kD centrosome autoantigen with a distinct cell cycle distribution. *J. Cell Biol.* 124:783–793.

Balczon, R., L. Bao, W.E. Zimmer, K. Brown, R.P. Zinkowski, and B.R. Brinkley. 1995. Dissociation of centrosome replication events from cycles of DNA synthesis and mitotic division in hydroxyurea-arrested Chinese hamster ovary cells. *J. Cell Biol.* 130:105–115.

Balczon, R., C.E. Varden, and T.A. Schroer. 1999. Role for microtubules in centrosome doubling in Chinese hamster ovary cells. *Cell Motil. Cytoskel.* 42:60–72.

Bernhard, W., and E. De Harven. 1960. L'ultrastructure du centriole et d'autres éléments de l'appareil achromatique. *In* Fourth International Conference on Electron Microscopy. W. Bargmann, D. Peters, and C. Wolpers, editors. Springer-Verlag, Berlin. 218–227.

Berns, M.W., J.B. Rattner, S. Brenner, and S. Meredith. 1977. The role of the centriolar region in animal cell mitosis. *J. Cell Biol.* 72:351–367.

Bessis, M., and J. Breton-Gorius. 1958. Sur une structure inframicroscopique pericentriolaire. Etude au microscope electronique sur les leucocytes des mammiferes. *C. R. Acad. Sci.* 246:1289.

Bornens, M., M. Paintrand, J. Berges, M.C. Marty, and E. Karsenti. 1987. Structural and chemical characterization of isolated centrosomes. *Cell. Motil. Cytoskel.* 8:238–249.

Brinkley, B.R. 1985. Microtubule organizing centers. *Annu. Rev. Cell Biol.* 1:145–172.

Cole, D.G., D.R. Diener, A.L. Himelblau, P.L. Beech, J.C. Fuster, and J.L. Rosenbaum. 1998. *Chlamydomonas* kinesis-II–dependent intraflagellar transport (IFT): IFT particles contain proteins required for ciliary assembly in *Caenorhabditis elegans* sensory neurons. *J. Cell Biol.* 141:993–1008.

de-Thé, G. 1964. Cytoplasmic microtubules in different animal cells. *J. Cell Biol.* 23:265–275.

Dirksen, E.R. 1991. Centriole and basal body formation during ciliogenesis revisited. *Biol. Cell.* 72:31–38.

Engelender, S., A.H. Sharp, V. Colomer, M.K. Tokito, A. Lanahan, P. Worley, E.L. Holzbaur, and C.A. Ross. 1997. Huntingtin-associated protein 1 (HAP1) interacts with the $p150^{Glued}$ subunit of dynactin. *Hum. Mol. Genet.* 6:2205–2212.

Fujimoto, T., S. Nakade, A. Miyawaki, K. Mikoshiba, and K. Ogawa. 1992. Localization of inositol 1,4,5-trisphosphate receptor-like protein in plasmalemmal caveolae. *J. Cell Biol.* 119:1507–1513.

Hyman, A., D. Drechsel, D. Kellogg, S. Salser, K. Sawin, P. Steffen, L. Wordeman, and T. Mitchison. 1991. Preparation of modified tubulins. *Methods Enzymol.* 196:478–485.

Kalt, A., and M. Schliwa. 1993. Molecular components of the centrosome. *Trends Cell Biol.* 3:118–128.

Kellogg, D.R., M. Moritz, and B.M. Alberts. 1994. The centrosome and cellular organization. *Ann. Rev. Biochem.* 63:639–674.

Kimble, M., and R. Kuriyama. 1992. Functional components of microtubule-organizing centers. *Int. Rev. Cytol.* 136:1–50.

Kozminski, K.G., K.A. Johnson, P. Forscher, and J.L. Rosenbaum. 1993. A motility in the eukaryotic flagellum unrelated to flagellar beating. *Proc. Natl. Acad. Sci. USA.* 90:5519–5523.

Laemmli, U.K. 1970. Cleavage of structural proteins during the assembly of the head of bacteriophage T4. *Nature.* 227:680–685.

Loots, G.P., and P.P.C. Nel. 1989. Early stages of ciliogenesis in the respiratory epithelium of the nasal cavity of rabbit embryos. *Cell Tissue Res.* 255:589–594.

Marshall, W.F., and J.L. Rosenbaum. 1999. Cell division: the renaissance of the centriole. *Curr. Biol.* 9:R218–R220.

Matulionis, D.H. 1975. Light and electron microscopic study of the effects of $ZnSO_4$ on mouse nasal respiratory epithelium and subsequent responses. *Anat. Rec.* 183:63–82.

Mitchison, T.J., and M.W. Kirschner. 1984. Microtubule assembly nucleated by isolated centrosomes. *Nature.* 312:232–237.

Mogensen, M.M., J.B. Tucker, and H. Stebbings. 1989. Microtubule polarities indicate that nucleation and capture of microtubules occurs at cell surfaces in *Drosophila*. *J. Cell Biol.* 108:1445–1452.

Ohta, K., N. Shiina, E. Okumura, S. Hisanaga, T. Kishimoto, S. Endo, Y. Gotoh, E. Nishida, and H. Sakai. 1993. Microtubule nucleating activity of centrosomes in cell-free extracts from *Xenopus* eggs: involvement of phosphorylation and accumulation of pericentriolar material. *J. Cell Sci.* 104: 125–137.

Rattner, J.B. 1992. Ultrastructure of centrosome domains and identification of their protein components. *In* The Centrosome. V.I. Kalnins, editor. Academic Press, Inc., San Diego, CA. 45–69.

Rhodin, J., and T. Dalhamn. 1956. Electron microscopy of the tracheal ciliated mucosa in rat. *Z. Zellforsch. Mikrosk. Anat.* 44:345–412.

Robbins, E., G. Jentzsch, and A. Micali. 1968. The centriole cycle in synchronized HeLa cells. *J. Cell Biol.* 36:329–339.

Rosenbaum, J.L., D.G. Cole, and D.R. Diener. 1999. Intraflagellar transport: the eyes have it. *J. Cell Biol.* 144:385–388.

Schroer, T.A., and M.P. Sheetz. 1989. Role of kinesin and kinesin-associated proteins in organelle transport. *In* Cell Movement. Vol. 2. F.D. Warner and J.R. McIntosh, editors. Alan R. Liss, Inc., New York. 295–306.

Shiina, N., T. Moriguchi, K. Ohta, Y. Gotoh, and E. Nishida. 1992. Regulation of a major microtubule-associated protein by MPF and MAP kinase. *EMBO (Eur. Mol. Biol. Organ.) J.* 11:3977–3984.

Shiina, N., and S. Tsukita. 1999. Mutations at phosphorylation sites of *Xenopus* microtubule-associated protein 4 affect its microtubule-binding ability and chromosome movement during mitosis. *Mol. Biol. Cell.* 10:597–608.

Smith, D.B., and K.S. Johnson. 1988. Single-step purification of polypeptides expressed in *Escherichia coli* as fusions with glutathione S-transferase. *Gene.* 67:31–40.

Sorokin, S.P. 1968. Reconstructions of centriole formation and ciliogenesis in mammalian lungs. *J. Cell Sci.* 3:207–230.

Steinman, R.M. 1968. An electron microscopic study of ciliogenesis in developing epidermis and trachea in the embryo of *Xenopus laevis*. *Am. J. Anat.* 122: 19–56.

Tokuyasu, K.T. 1980. Immunochemistry on ultrathin frozen sections. *Histochem. J.* 12:381–403.

Vandré, D.D., and G.G. Borisy. 1989. The centrosome cycle in animal cells. *In* Mitosis: Molecules and Mechanisms. J.S. Hyams and B.R. Brinkley, editors. Academic Press, San Diego, CA. 39–75.

Wittmann, T., H. Boleti, C. Antony, E. Karsenti, and I. Vernos. 1998. Localization of the kinesin-like protein Xklp2 to spindle poles requires a leucine zipper, a microtubule-associated protein, and dynein. *J. Cell Biol.* 143:673–685.

Yonemura, S., M. Itoh, A. Nagafuchi, and S. Tsukita. 1995. Cell-to-cell adherens junction formation and actin filament organization: similarities and differences between non-polarized fibroblasts and polarized epithelial cells. *J. Cell Sci.* 108:127–142.

Youson, J.H. 1982. Replication of basal bodies and ciliogenesis in a ciliated epithelium of the lamprey. *Cell Tissue Res.* 223:255–266.

Zimmerman, W., C.A. Sparks, and S.J. Doxsey. 1999. Amorphous no longer: the centrosome comes into focus. *Curr. Opin. Cell Biol.* 11:122–128.

Figure 7. Localization of mPCM-1 in nasal respiratory epithelial cells at four days after exposure to distilled water (a–c) or irritation with 1% aqueous $ZnSO_4$ (d–f). a, Conventional ultrathin EM. Electron-dense spherical granules (arrowheads), ~70–100 nm in diameter, which were morphologically indistinguishable from centriolar satellites, were scattered close to ciliary basal bodies (asterisks). Open arrows, microtubules. b, Preembedding immunoelectron microscopy. Nasal epithelial tissues were treated with 0.5% Triton X-100, fixed with glutaraldehyde, then labeled with anti–mPCM-1 pAb. The centriolar satellite-like granules were specifically labeled (arrowheads). c, Postembedding immunoelectron microscopy. Ultrathin cryosections of nasal epithelial cells were labeled with anti–mPCM-1 pAb. The centriolar satellite-like granules were specifically labeled (arrowheads). d, Conventional ultrathin EM. Cilia were completely removed, and at the apical cytoplasm numerous fibrous granules (arrowheads), as well as deuterosomes (arrows), appeared. e, Preembedding immunoelectron microscopy. Samples were treated with 0.5% Triton X-100, fixed with glutaraldehyde, then labeled with anti–mPCM-1 pAb. Fibrous granules (arrowheads), but not deuterosomes (arrow), were heavily labeled. Both centriolar and acentriolar pathways for centriolar replication were observed (see details in the text). f, Postembedding immunoelectron microscopy. Ultrathin cryosections were labeled with anti–mPCM-1 pAb. Fibrous granules (arrowheads), but not deuterosomes (arrow), were specifically labeled. Bars, 200 nm.